HHS Public Access

Author manuscript

Neuroimage. Author manuscript; available in PMC 2018 March 01.

Published in final edited form as:

Neuroimage. 2017 March 01; 148: 296–304. doi:10.1016/j.neuroimage.2016.12.026.

In vivo Detection of Microstructural Correlates of Brain Pathology in Preclinical and Early Alzheimer Disease with Magnetic Resonance Imaging

Yue Zhao[1], **Marcus E. Raichle**[2,3], **Jie Wen**[2], **Tammie L. Benzinger**[2], **Anne M. Fagan**[3,4], **Jason Hassenstab**[3,4], **Andrei G. Vlassenko**[2], **Jie Luo**[2], **Nigel J. Cairns**[3,4], **Jon J. Christensen**[2], **John C. Morris**[3,4], and **Dmitriy A. Yablonskiy**[2,*]

[1]Department of Chemistry, Washington University in St. Louis, St. Louis, MO 63110, USA

[2]Department of Radiology, Washington University in St. Louis, St. Louis, MO 63110, USA

[3]Department of Neurology, Washington University in St. Louis, St. Louis, MO 63110, USA

[4]Knight Alzheimer's Disease Research Center, Washington University in St. Louis, St. Louis, MO 63110, USA

Abstract

Background—Alzheimer disease (AD) affects at least 5 million individuals in the USA alone stimulating an intense search for disease prevention and treatment therapies as well as for diagnostic techniques allowing early identification of AD during a long pre-symptomatic period that can be used for the initiation of prevention trials of disease-modifying therapies in asymptomatic individuals.

Methods—Our approach to developing such techniques is based on the Gradient Echo Plural Contrast Imaging (GEPCI) technique that provides quantitative *in vivo* measurements of several brain-tissue-specific characteristics of the gradient echo MRI signal (GEPCI metrics) that depend on the integrity of brain tissue cellular structure. Preliminary data were obtained from 34 participants selected from the studies of aging and dementia at the Knight Alzheimer's Disease Research Center at Washington University in St. Louis. Cognitive status was operationalized with the Clinical Dementia Rating (CDR) scale. The participants, assessed as cognitively normal (CDR = 0; n = 23) or with mild AD dementia (CDR = 0.5 or 1; n = 11) underwent GEPCI MRI, a collection of cognitive performance tests and CSF amyloid (Aβ) biomarker $A\beta_{42}$. A subset of 19 participants also underwent PET PiB studies to assess their brain Aβ burden. According to the Aβ status, cognitively normal participants were divided into normal (Aβ negative; n = 13) and preclinical (Aβ positive; n = 10) groups.

*Corresponding Author: Dmitriy A. Yablonskiy Mallinckrodt Institute of Radiology, Washington University, 4525 Scott Ave. Room 3216, St. Louis MO, 63110. Tel.: +1(314)362-1815; Fax: +1(314)362-0526. yablonskiyd@wustl.edu.

Results—GEPCI quantitative measurements demonstrated significant differences between all the groups: normal and preclinical, normal and mild AD, and preclinical and mild AD. GEPCI quantitative metrics characterizing tissue cellular integrity in the hippocampus demonstrated much stronger correlations with psychometric tests than the hippocampal atrophy. Importantly, GEPCI-determined changes in the hippocampal tissue cellular integrity were detected even in the hippocampal areas not affected by the atrophy. Our studies also uncovered strong correlations between GEPCI brain tissue metrics and beta-amyloid (Aβ) burden defined by positron emission tomography (PET) - the current *in vivo* gold standard for detection of cortical Aβ, thus supporting GEPCI as a potential surrogate marker for Aβ imaging – a known biomarker of early AD. Remarkably, the data show significant correlations not only in the areas of high Aβ accumulation (e.g. precuneus) but also in some areas of medial temporal lobe (e.g. parahippocampal cortex), where Aβ accumulation is relatively low.

Conclusion—We have demonstrated that GEPCI provides a new approach for the *in vivo* evaluation of AD-related tissue pathology in the preclinical and early symptomatic stages of AD. Since MRI is a widely available technology, the GEPCI surrogate markers of AD pathology have a potential for improving the quality of AD diagnostic, and the evaluation of new disease-modifying therapies.

Keywords

Alzheimer’s disease; MRI; PET; beta-amyloid; pathology; GEPCI

INTRODUCTION

Alzheimer disease (AD) is a neurodegenerative disorder that is characterized by intraneuronal aggregates of tau called neurofibrillary tangles and extracellular aggregates of amyloid-beta (Aβ) protein called plaques. Clinically, AD is characterized by memory deficits and progressive cognitive impairment leading to dementia. To date all disease-modifying experimental therapies for AD have failed to demonstrate clinical benefit in individuals with symptomatic AD (1,2), possibly because the drugs were administered too late in the course of the disease which begins 15–20 years prior to the onset of clinical symptoms (3–10). This preclinical stage of AD provides a large window for therapeutic intervention (11). Hence, one of the important directions in AD therapy is developing widely accessible neuroimaging techniques that can detect AD brain pathology in the preclinical stages (12,13).

One of the prevailing hypotheses of AD is the amyloid cascade hypothesis (3,5–7) that suggests that abnormal accumulation of (Aβ) in the neocortex is one of the earliest pathological markers of AD. Paradoxically, it is also known that the medial temporal lobe (MTL), a region that mediates short-term memory, is affected early in the disease but is not the most affected region by Aβ deposition compared with neocortical regions (e.g. prefrontal cortex and precuneus (14–16)). At the same time, histological studies show that the MTL is particularly vulnerable to neurofibrillary pathology in the early stages of aging and AD (17–22). The reduction of volume and the loss of cells in the entorhinal cortex and hippocampus have been extensively reported in participants with mild cognitive impairment (MCI) and

AD (23–27). Importantly, neuropathology studies have established that symptomatic AD begins only when cell loss occurs in the hippocampal area (25).

MRI is a potentially powerful tool to identify changes in the Alzheimer brain. Most MRI studies so far have focused on AD-related volumetric measurements of brain atrophy (28). A few studies attempted to identify plaques via MRI in postmortem specimens or mice models (29–34), though the latter methods require long imaging time and have not been translated to human studies.

In this paper we use an MRI-based method allowing *in vivo* simultaneous detection of Aβ accumulation and cellular damage in humans with Alzheimer disease. Our approach is based on the Gradient Echo Plural Contrast Imaging (GEPCI) technique (35–37) previously used in normal aging studies (38) and to identify brain tissue damage in multiple sclerosis (35,36,39–42) and psychiatric diseases (43). The GEPCI technique provides quantitative *in vivo* high resolution 3D measurements of several brain-tissue-specific parameters of the gradient recalled echo MRI signal (GEPCI metrics - see specific definitions in the next section). The GEPCI metrics depending on the molecular constituents of cell-building materials present in the brain (38) can serve as surrogate markers reflecting disease-related tissue damage.

The goal of this study was to establish the relationship between GEPCI metrics and AD-related tissue damage at preclinical and very early symptomatic stages of AD. To this end, we enrolled participants from the Washington University Knight Alzheimer's Disease Research Center (Knight ADRC) with well-characterized clinical status ranging from cognitively normal to very mild and mild AD, and with a battery of psychometric, CSF and neuroimaging data. We demonstrated a significant correlation between GEPCI metrics of brain tissue cellular damage in the hippocampus and cognitive performance. Importantly, this correlation is stronger than the correlation between cognitive performance and hippocampal atrophy, thus suggesting that the integrity of the remaining tissue is a more important parameter for brain functioning than the loss of tissue volume alone. We also uncovered a remarkable correlation between GEPCI metrics and β-amyloid load measured by positron emission tomography (PET) (the current *in vivo* gold standard), thus supporting GEPCI as a potential surrogate marker for Aβ imaging in preclinical and early Alzheimer disease.

Our results demonstrate that GEPCI is sensitive to early AD-related pathological changes in brain tissue. Since our approach is based on MRI that is widely available worldwide, is non-invasive, and does not require radiation exposure, it can open opportunities for obtaining new information on the pathogenesis of AD, one of the most devastating diseases of older adults. The new method can also open the door for screening cohorts for clinical drug trials that are enrolling individuals with preclinical or early symptomatic AD.

METHODS

Participants

This study was approved by the Institutional Review Board of Washington University School of Medicine (WUSM). 34 participants were selected from the studies of aging and dementia at the Knight Alzheimer's Disease Research Center (ADRC) at WUSM. All participants provided informed consent. Cognitive status was operationalized with the Clinical Dementia Rating (CDR) (44), as determined by Knight ADRC clinicians according to standard protocols; diagnoses were in accordance with standard criteria (2). The participants were assessed to be cognitively normal (CDR = 0) or to have mild (CDR = 0.5 or 1) AD dementia. All participants in this study underwent a collection of cognitive performance tests (45), including Free and Cued Selective Reminding Test (Srtfree), Animal Naming (ANIMALS), and Trail making Test Part A (Tma). CSF biomarker $A\beta_{42}$ (INNOTEST, Fujirebio, Gent, Belgium) was available for 31 participants. 19 participants underwent PiB PET imaging to estimate amyloid deposition in their brains. According to the Aβ status (see below), cognitively normal participants (CDR = 0) were divided into normal (CDR = 0; Aβ negative) and preclinical (CDR = 0; Aβ positive) groups. Demographic information for all groups is presented in Table 3. For participants that underwent PET amyloid imaging, amyloid positivity was defined by a cutoff of mean cortical binding potential (MCBP)=0.18 (46) which corresponds to a mean cortical standardized uptake value ratio (MC-SUVR) of 1.3 referenced to cerebellar grey matter. MC-SUVR for Aβ imaging is calculated as the average of regions within the prefrontal cortex, gyrus rectus, lateral temporal, and precuneus regions. For participants that did not have PET Aβ measurements, Aβ positivity was determined by the status of their CSF biomarker $A\beta_{42}$ (12). One participant with CDR = 0.5 and one with CDR = 1 had negative Aβ status.

MRI Data Acquisition

All participants were scanned in a 3T PET-MR scanner (Siemens, Erlangen, Germany). A 3D multi gradient echo sequence was used to obtain the data. Sequence parameters were: resolution 1×1×2 mm^3 (read, phase, slab), FOV 256 mm×192 mm, repetition time TR = 50ms, flip angle 30°, 10 gradient echoes with first gradient echo time TE_1 = 4 ms, echo spacing ΔTE = 4ms. Additional phase stabilization echo (the navigator data) was collected for each line in k-space to correct for image artifacts due to the physiological fluctuations (40). The total acquisition time of GEPCI was 11 mins 30s. Macroscopic field inhomogeneity effects (background gradients) were accounted for by using the voxel spread function (VSF) approach (47). Standard clinical Magnetization-Prepared Rapid Gradient Echo (MPRAGE) (48) images with TR/TI/TE = 2200/1100/3.37 ms and the resolution 1×1×1 mm^3 were also collected for segmentation purposes. The total acquisition time of MPRAGE is 6 mins.

Data Analysis and GEPCI Images Generation

After data acquisition, raw k-space data were read into MATLAB (The MathWorks, Inc.) for postprocessing using previously developed algorithms (36,37,40,47). In brief, after correcting the k-space data for physiological artefacts (40), we applied FFT to get images. 3D spatial Hanning filter was then applied to the data in the image domain to reduce Gibbs

ringing artefacts and increase signal-to-noise ratio (SNR) in the data. The multi-channel data were combined using the following algorithm (36):

$$S_n(TE)=\sum_{ch=1}^{M}\lambda_{ch}\cdot\overline{S}_n^{ch}(TE_1)\cdot S_n^{ch}(TE);\quad \lambda_{ch}=\frac{1}{M\cdot\varepsilon_{ch}^2}\sum_{ch'=1}^{M}\varepsilon_{ch'}^2 \qquad [1]$$

where the sum was taken over all M channels (ch), $\bar{S}$ denotes complex conjugate of S, λ_{ch} are weighting parameters and ε_{ch} are noise amplitudes (r.m.s.). Index n corresponds to the voxel position (n=x,y,z). As we demonstrated previously, this algorithm allows for the optimal estimation of quantitative parameters (36,49), and also removes the initial phase incoherence among the channels (36).

Standard R2* = 1/T2* values will be estimated by fitting the following equation to experimental data:

$$S(TE)=A_0\cdot\exp\left(-R2^*\cdot(TE+TE_1)+i\cdot 2\pi\cdot\Delta f\cdot(TE-TE_1)\cdot F(TE)\right) \qquad [2]$$

where TE is the gradient echo time, Δf is the frequency shift (dependent on tissue structure and also macroscopic magnetic field created mostly by tissue/air interfaces), and function F(TE) describes the effects of macroscopic magnetic field inhomogeneities (50). We use a voxel spread function (VSF) method (47) for calculating F(TE).

To separate contributions of tissue-specific (*R2t**) and susceptibility effects (50,51) to the total *R2** relaxation, we use the theoretical model (50,51) that we have developed previously:

$$S(TE)=A_0\cdot\exp\left[-R2t^*\cdot(TE+TE_1)-\zeta\cdot f_s(\delta\omega\cdot TE)+i\cdot 2\pi\cdot\Delta f\cdot(TE-TE_1)\right]\cdot F(TE)$$

[3]

where ζ is the volume fraction of magnetic susceptibility inclusions, $\delta\omega$ is the characteristic frequency determined by the susceptibility difference between inclusions and surrounding tissue (51), and non-linear function f_s defined in (51), describes the signal decay due to the presence of magnetic susceptibility inclusions. This model can account for different types of inclusions, e.g. blood vessel network (BOLD effect), trabecular bone, iron oxide nanoparticles, etc. (51). In this paper we use it for modeling transverse relaxation of GRE signal created by amyloid plaques that are known to create *R2** signal decay (34). Since no correlation exists between amyloid accumulation and BOLD effect (52), the correlation between amyloid accumulation and *R2**, that we found in AD patients (see preliminary data), is mostly related to magnetic susceptibility effects created by amyloid plaques. A hypothesized iron deposition in amyloid plaques (30,53) could lead to additional sensitivity of GEPCI *R2** to Aβ accumulation.

By fitting equation [3] to the complex signal using nonlinear regression algorithm, we are able to find the five parameters: A_0, $R2t^*$, Δf, ζ and $\delta\omega$ for each voxel in the brain. Details of the fitting routine are described in great detail in (37). The accuracy of parameter estimation was provided in (54) and (38).

In this application we focus on total $R2^*$ and tissue specific $R2t^*$ measurements for quantifying tissue microstructural properties and GEPCI T1W images (the square root of parameter A_0 in Eqs. [2], [3]) for brain structure delineation and segmentation.

Image segmentation

FreeSurfer software (Laboratory for Computational Neuroimaging, Martinos Center for Biomedical Imaging) (55) was used to generate brain segmentations, calculate surfaces, cortical thicknesses and volumes based on MPRAGE images. Then, MPRAGE images are registered to GEPCI-T1-weighted (T1W) images using FMRIB's Linear Image Registration Tool (56,57) in FSL and the transformation matrices of the registration are generated. Finally, these matrices were applied to the brain segmentations from FreeSurfer and transformed to the space of GEPCI-T1W images. One of the important advantages of GEPCI is that all GEPCI images are generated from a single MRI scan and are naturally co-registered. Hence, segmentations of GEPCI T1W images were naturally co-registered with all other GEPCI maps. To minimize the partial volume effect we applied a CSF mask to remove CSF signals. To maximize accuracy of measurements we report statistical results instead of voxel-wise analysis: for each FreeSurfer region (usually containing thousands of voxels), we generated a single parameter – mean value of GEPCI parameter.

RESULTS AND DISCUSSION

GEPCI technique is based on (**i**) 3D Gradient Recalled Echo (GRE) MRI sequence with multiple gradient echoes (currently available from most MRI scanner manufacturers), (**ii**) theoretical model of GRE signal relaxation properties (51), and (**iii**) a set of post-processing algorithms (36,37,40,47,58) allowing generating images and quantitative maps with several contrasts reflecting biological tissue anatomic, microstructural and functional properties. Importantly, all these GEPCI images are simultaneously acquired thus are naturally co-registered. Our theoretical model (51) is broadly accepted for GRE signal analysis. We have validated it on phantoms (50) and a small animal model (59), developed algorithms for correction of adverse background field gradient effects (47) and a method for minimizing effects of physiological fluctuations (40). The accuracy analysis was provided in (54) and (38).

The GEPCI technique (35–37) mainly relies on the quantitative measurements of the transverse relaxation properties (T2*) of the GRE MRI signal. The tissue MRI relaxation parameters measured by GEPCI depend on the cellular environment of water molecules – higher concentrations of proteins, lipids, iron, and other constituents of biological tissue and cell-building materials (sources of MR signal relaxation) lead to higher relaxation rate constants. Indeed, in a pure water or CSF, the $R2^*$ (=1/T2*) is about 1 s^{-1}, while in a normal brain tissue $R2^*$ is about 15–20 s^{-1}. A novel advanced approach that we developed (37) allows us to separate the total $R2^*$ relaxation into a tissue-specific ($R2t^*$) and susceptibility

effects. Since R2t* describes the part of the signal decay resulting from water molecules interaction with cellular components of biological tissues, it is sensitive to cellular alterations in human brain (37,38).

In the context of AD, we hypothesize that increased beta-amyloid deposition should lead to an increase in GEPCI metrics, especially R2* that is sensitive to mesoscopic field inhomogeneities (50,51) that can be present around amyloid deposits and can be enhanced due to the presence of iron in amyloid plaques (30). On the other hand, cellular loss characteristic of AD can lead to decreased GEPCI metrics, especially R2t* that is sensitive to cellular structure (38). The interplay between these two opposing processes can define important features of the GEPCI signal in AD.

In this paper we studied older adult participants, including those without AD symptoms and those with very mild/mild symptomatic AD. The most prominent pathological changes in the GEPCI metrics were found mostly in the MTL, an area affected early in AD.

Correlation between R2* and PET Aβ measurement

The correlation analysis between GEPCI measurements of R2* relaxation rate constant and amyloid PET measurements (using PiB standardized uptake value ratio [SUVR]) revealed positive correlations in most cortical brain regions. The data show significant correlations not only in the areas of high Aβ accumulation (e.g. precuneus) but also in the areas of MTL, such as the parahippocampal cortex and the fusiform cortex. While most brain regions demonstrated positive correlation between GEPCI R2* and PET amyloid SUVR, not all correlations were statistically significant after correction for multiple comparison using false discovery rate (FDR) (60), most likely due to the small sample size (PiB data were available only for 19 participants). Examples of the correlations with significant p values are shown in Figure 1.

The strongest correlation between GEPCI R2* and Aβ SUVR that we found in the parahippocampal cortex shows the high sensitivity of GEPCI R2* to Aβ accumulation in this area.

Interestingly, although the range of SUVR in parahippocampal cortex is smaller than in precuneus, the correlation in parahippocampal cortex is much stronger than that in precuneus. It indicates that even though MTL is not the area of the highest burden of Aβ in the AD brain, it represents a very important area of pathological changes in early AD particularly as it relates to the formation of Aβ plaques in the cerebral cortex, where the changes can be detected by GEPCI R2*. This feature likely can be attributed to distinct cellular properties of the gray matter in the MTL that play important roles in functionally connecting the neocortex and hippocampus (61). Structurally, the parahippocampal gyrus is a transitional zone, where the entorhinal cortex (referred as perialocortex) contains the lamina dissecans while the perirhinal and parahippocampal cortexes (referred as proisocortex) have their cellular structure different from the major three-layered and six-layered cortex areas (62). As different cellular components and arrangements contribute to R2*, it is possible that the strong correlations between R2* and Aβ SUVR in the parahippocampal cortex is due to its unique laminar organizations. Since the medial portion

of the fusiform gyrus is also considered to be part of the parahippocampal cortex, it is reasonable to observe the significant correlation between R2*and Aβ SUVR in the fusiform as well.

The presence of neurofibrillary tangles (NFTs) and neuronal loss in the parahippocampal gyrus previously reported by Thangavel *et al* (22) can also affect R2* measurements. However, their participants were assessed at death after nearly a decade of dementia, while the cohort in our study represents mostly normal, pre-symptomatic, very mild (CDR = 0.5) or mild (CDR=1) AD. In addition, as tissue damage in the parahippocampal gyrus was smaller than that in the hippocampus (20), in our cohort the loss of neurons in the parahippocampal gyrus may not be severe enough to affect our R2* measurements.

Even though the significance of local correlations between R2*and Aβ SUVR vary for different brain regions, our R2* measurements in the parahippocampal cortex (area of the strongest local correlation between Aβ SUVR and R2*) can still be used for evaluation of Aβ burden in all multiple regions. Indeed, our data show very strong correlations between Aβ SUVR in most cortical regions and the R2*values in the parahippocampal cortex. These correlations can be described as follows:

$$SUVR = a + k \cdot (R2^*_{PH} - \overline{R2}^*_{PH}) \quad [4]$$

and can be used for evaluation of Aβ SUVR for a given participant in any cortical region. In Eq. [4], the $R2^*_{PH}$ is the parahippocampal $R2^*$ value for a given participant, $\overline{R2}^*_{PH} = 16.55\,\mathrm{sec}^{-1}$, is the mean value of R2*in the parahippocampal cortex of the normal control group (9 participants with negative PiB Aβ and CDR = 0). The coefficients *a* and *k* in Eg. [4], specific for each cortical region, are provided in Table 1 along with the results of correlation analysis. The $\overline{R2}^*_{PH}$ is introduced in Eq. [4] to make the coefficients *a* of the regression analysis more meaningful – in Eq. [4] they represent region-specific average SUVR values for healthy control group. The slopes of the regression (parameter *k* in Eq.[4]) are also shown in Fig. 2, upper row. The spatial pattern in Figure 2 is similar to previously established correlation pattern between regional and mean values of PiB SUVR (63). Hence, our data demonstrate that the R2*measurements in the MTL (especially the parahippocampal cortex) not only correlate with amyloid PET measurements in this area but also strongly correlate with amyloid PET measurements throughout the entire cortex.

While our data show rather significant positive correlations between R2* and amyloid burden across the participants in different brain regions (Figure 1), there also exists an *inverse association* across the brain regions between averaged R2* and amyloid distributions. Figure 2 shows mean values of R2* and Aβ SUVR averaged across 19 participants mapped onto the brain surface. Lower R2* are found in the frontal cortex, posterior cingulate, precuneus, parahippocampal cortex, entorhinal cortex and superior temporal cortex. Higher R2* are found in the occipital cortex, paracentral cortex, fusiform, middle and inferior temporal cortex. This R2* distribution is consistent with the previous studies (38). In contrast to the R2*, the PiB retention was prominently higher in the frontal

cortex, posterior cingulate, precuneus and inferior parietal cortex, which is also consistent with the previous reports (9,15). Generally speaking, PiB Aβ binding tends to increase in the regions with lower R2*, which may indicate that the regions with lower R2* are more vulnerable to the amyloid accumulation. This relationship is more obvious on the map in the frontal cortex, posterior cingulate, precuneus, inferior parietal cortex characterized with higher SUVR but lower R2*, and occipital cortex with lower SUVR but higher R2*. Interestingly, the former regions mostly overlap the default mode network (64) and tend to be both structurally and functionally vulnerable in normal aging and Alzheimer's disease, which was suggested to be due to a high degree of life-long plasticity (65). The R2*-Aβ association points to an important relationship between brain microstructural properties reflected in tissue specific R2* measurements and the relationships between default activity, amyloid, and memory previously reported by Buckner et al (66). It is also in agreement with our previous consideration (38) that the cortical areas with lower R2t* (e.g. prefrontal cortex) may have more complex dendritic and synaptic structure, which may also be related to the neuroplasticity and AD vulnerability. From this perspective, the parahippocampal and entorhinal cortices, which are primary memory-related areas and are vulnerable to early Alzheimer, are also characterized by a lower baseline R2*. However, PiB retention and Aβ accumulation in these areas are not prominent. Nevertheless, the correlation between GEPCI R2* metrics and PiB retention in these areas is exceptionally strong, especially in the parahippocampal gyrus.

R2* provides differentiation between normal and preclinical AD participants

Based on PET PiB and GEPCI measurements available for 19 participants of our study, we have uncovered strong correlations between Aβ SUVR and R2* measurements in many cortical brain regions (see Figure 1). Since early AD is associated with Aβ accumulation (3,5–7), this suggests that the R2* can potentially be used to differentiate between healthy and preclinical AD stages. Indeed, Figure 3 shows statistically significant differences based on R2* measurements in the parahippocampal cortex between amyloid negative and positive groups of our 34 participants (recall that two CDR positive participants were Aβ negative). The bar graph on the left in Figure 3 shows a significant difference in the parahippocampal R2* between all participants (independent of CDR) with negative (n = 15) and positive (n = 19) Aβ status (see definition in the Methods). The bar graph on the right shows significant differences between normal group (CDR = 0, amyloid negative, n=13) and preclinical group (CDR = 0, Aβ positive, n = 10).

Correlation between R2t* and cognitive performance tests

Previously (38), we compared GEPCI-derived tissue specific structural and functional metrics with existing literature and hypothesized that the parameter R2t* is related to the tissue neuronal density. Since our participants were characterized either as cognitively normal or having mild cognitive impairment (MCI), we found very few differences in their R2t* in most brain areas with the exception of the hippocampus. Importantly, the hippocampal R2t* correlated significantly with cognitive performance (Figure 4), which is not surprising because a decreased R2t* in the hippocampus is related to decreased neuronal density. As presented in the scatter plots in Figure 4, the hippocampal R2t* was associated with the free recall condition of the Free and Cued Selective Reminding Test (Srtfree; r =

0.53, p = 0.002), with the total correct score from the Animal Naming test (ANIMALS; r = 0.50, p = 0.0025), and with the Trailmaking Test Part A completion time (Tma; r = −0.47, p > 0.017).

Note that considerably weaker correlations were found between hippocampal volume and cognitive performance (Figure 4, second column), suggesting that the integrity of the remaining hippocampal tissue (characterized by R2t*) is a more important parameter of hippocampal pathology than hippocampal volume.

No significant correlation was found between cognitive performance and R2* or CSF $A\beta_{42}$. This result is in agreement with the dissociation between PiB defined Aβ plaques and cognitive performance (67–71). At least 30% of people with significant Aβ burden are cognitively normal (67).

R2t* provides differentiation between cognitively normal and mild AD groups

Figure 5 shows examples of GEPCI images obtained from three participants representing healthy control, preclinical and mild AD groups. Thin yellow contour outlines hippocampal area determined by FreeSurfer segmentation. In all cases, MPRAGE and GEPCI T1w images show small atrophy progressing from healthy to AD group. Gradually decreased GEPCI R2t* suggest altered tissue integrity even in the preserved hippocampal area. One should keep in mind that GEPCI metrics (R2* and R2t*) are quantitative and provide information on tissue integrity based on comparison with healthy control measurements, thus uncovering tissue damage that might not be simply visible on images. Though tissue damage in the hippocampus can be clearly seen as hypointense signal on R2t* maps.

While changes in R2t* likely reflect changes in the neuronal and synaptic density, it may also reflect changes in other tissue components. Hypothetically, a small (not significant) increase in tissue R2t* seen in preclinical group as compared to normal participants may be attributed to accumulation of tau protein as in early Braak stages (17) of AD. Interestingly, the hippocampal volume in the preclinical group was also slightly (not significant) higher than in the normal group.

The bar graphs in Figure 6 show group comparisons based on the R2t* results obtained in the hippocampus. Three groups are shown - normal participants (CDR = 0, Aβ negative), preclinical group (CDR = 0, Aβ positive) and mild AD (CDR = 0.5 or 1). The first box shows results for tissue R2t* and the second block shows results for hippocampal volume. The significantly decreased hippocampal volume in mild AD group is in agreement with known brain atrophy characteristic for AD (28).

If R2t* is related to neuronal density/integrity, the product of R2t* and the hippocampal volume (V) could characterize the total neuronal content in the hippocampus. Hence, to characterize the global tissue change in the hippocampus, it is convenient to introduce the Tissue Content Index (TCI):

$$TCI = \frac{(V \cdot R2t^*) - (V \cdot R2t^*)_{control}}{(V \cdot R2t^*)_{control}} \quad [5]$$

where $(V \cdot R2t^*)_{control}$ =41201 $mm^3 \cdot sec^{-1}$ is a mean value of tissue content in the group of normal participants. The changes in the TCI between Normal, Preclinical and AD groups are shown in the third box of Figure 6.

The results in Figure 6 (hippocampal data) show that not only is the hippocampal tissue volume reduced in mild AD participants, but the tissue specific R2t* value is also reduced. It is not surprising that the TCI representing the product of the volume and R2t*, is reduced even more significantly. These results are in a full agreement with the histopathological studies of Price, Morris and co-workers (25) who found that 46% of neurons were lost in the hippocampus of people with CDR = 0.5 as compared to cognitively normal participants, while the hippocampal volume loss was only 29%. Comparison of our findings with direct neuronal measurements in (25) further confirms our hypothesized relationship between R2t* and neuronal density. The decreased R2t* and TCI is consistent with decreased tissue neuronal density and the tissue neuronal content in the hippocampus. Furthermore, no significant differences in hippocampal R2t*, volume and TCI between the normal and preclinical AD groups, is also consistent with Price, Morris and co-workers' finding of no significant difference in hippocampal neuron number and volume between the normal and preclinical AD groups (25).

The results of this study are based on data obtained from 34 participants. Larger and independent samples certainly should be used to further validate our findings.

Last but not least, the GEPCI approach has been used previously to study normal aging (38) and to identify brain tissue damage in multiple sclerosis (35,36,39–42) and psychiatric diseases (43). In the normal aging study (38), a significant increase of R2* and R2t* with age was found in most brain regions. We hypothesized that the age-related increased R2t* in the cerebral cortex was consistent with increased neuronal density, which is supported by various histological studies showing no significant change of the total number of neurons but significant decrease of brain volume over age (see references in (38)). Furthermore, R2* values were found to be significantly lower in patients with multiple sclerosis (MS) compared with healthy participants (35,36,39–42). Significant correlations between age-adjusted R2* measurements and clinical scores of MS were also reported in cortical regions (41). Significant group effects based on GEPCI measurements were observed in the superior temporal cortex and the thalamus in participants with schizophrenia and bipolar disorder (43).

CONCLUSION

In this paper we have demonstrated that the GEPCI technique provides a new approach to the *in vivo* evaluation of pathology in the preclinical and early symptomatic stages of AD. It is based on a multi-gradient-echo MRI sequence that is available from most MRI manufacturers. GEPCI data are quantitative, reproducible and MRI scanner independent,

thus allowing multi-center applications. Our results show that GEPCI metrics are good correlates of Aβ accumulation and neurodegeneration. They are sensitive enough to distinguish between normal individuals and those with preclinical (asymptomatic) and early symptomatic AD.

One of the significant conclusions of our study is that the tissue cellular integrity of the preserved part of the hippocampus is a more important parameter affecting cognitive performance than the hippocampal atrophy. This points out to the presence of significant cognitive reserve in the hippocampal structure. Another important finding is that the AD symptoms do not start until there has been significant cellular loss in the hippocampus identified by GEPCI metrics, consistent with Price, Morris and colleagues (25).

Since MRI is a much more available modality than PET (current imaging "gold standard" for *in vivo* quantifying AD (Aβ) brain pathology), and poses fewer risks, GEPCI metrics (R2* and R2t*) have a potential for improving the quality of AD diagnostic measures, and the evaluation of new disease-modifying therapies.

Acknowledgments

Research reported in this publication was supported by the Washington University Institute of Clinical and Translational Sciences grant UL1 TR000448 from the NIH National Center for Advancing Translational Sciences and NIH grants P50AG05681 and P01AG03991. We would also like to thank Dr. Astafiev for helpful discussion.

References

1. Albert MS, DeKosky ST, Dickson D, Dubois B, Feldman HH, Fox NC, Gamst A, Holtzman DM, Jagust WJ, Petersen RC, Snyder PJ, Carrillo MC, Thies B, Phelps CH. The diagnosis of mild cognitive impairment due to Alzheimer's disease: Recommendations from the National Institute on Aging-Alzheimer's Association workgroups on diagnostic guidelines for Alzheimer's disease. Alzheimer's & Dementia. 2011; 7(3):270–279.
2. McKhann GM, Knopman DS, Chertkow H, Hyman BT, Jack CR Jr, Kawas CH, Klunk WE, Koroshetz WJ, Manly JJ, Mayeux R, Mohs RC, Morris JC, Rossor MN, Scheltens P, Carrillo MC, Thies B, Weintraub S, Phelps CH. The diagnosis of dementia due to Alzheimer's disease: Recommendations from the National Institute on Aging-Alzheimer's Association workgroups on diagnostic guidelines for Alzheimer's disease. Alzheimer's & Dementia. 2011; 7(3):263–269.
3. Selkoe DJ. Alzheimer's disease. In the beginning Nature. 1991; 354(6353):432–433.
4. Hardy J, Allsop D. Amyloid deposition as the central event in the aetiology of Alzheimer's disease. Trends Pharmacol Sci. 1991; 12(10):383–388. [PubMed: 1763432]
5. Hardy JA, Higgins GA. Alzheimer's disease: the amyloid cascade hypothesis. Science. 1992; 256(5054):184–185. [PubMed: 1566067]
6. Hardy J, Selkoe DJ. The amyloid hypothesis of Alzheimer's disease: progress and problems on the road to therapeutics. Science. 2002; 297(5580):353–356. [PubMed: 12130773]
7. Jack CR Jr, Knopman DS, Jagust WJ, Shaw LM, Aisen PS, Weiner MW, Petersen RC, Trojanowski JQ. Hypothetical model of dynamic biomarkers of the Alzheimer's pathological cascade. The Lancet Neurology. 2010; 9(1):119–128. [PubMed: 20083042]
8. Bateman RJ, Xiong C, Benzinger TL, Fagan AM, Goate A, Fox NC, Marcus DS, Cairns NJ, Xie X, Blazey TM, Holtzman DM, Santacruz A, Buckles V, Oliver A, Moulder K, Aisen PS, Ghetti B, Klunk WE, McDade E, Martins RN, Masters CL, Mayeux R, Ringman JM, Rossor MN, Schofield PR, Sperling RA, Salloway S, Morris JC. Dominantly Inherited Alzheimer N. Clinical and biomarker changes in dominantly inherited Alzheimer's disease. The New England journal of medicine. 2012; 367(9):795–804. [PubMed: 22784036]

9. Benzinger TL, Blazey T, Jack CR Jr, Koeppe RA, Su Y, Xiong C, Raichle ME, Snyder AZ, Ances BM, Bateman RJ, Cairns NJ, Fagan AM, Goate A, Marcus DS, Aisen PS, Christensen JJ, Ercole L, Hornbeck RC, Farrar AM, Aldea P, Jasielec MS, Owen CJ, Xie X, Mayeux R, Brickman A, McDade E, Klunk W, Mathis CA, Ringman J, Thompson PM, Ghetti B, Saykin AJ, Sperling RA, Johnson KA, Salloway S, Correia S, Schofield PR, Masters CL, Rowe C, Villemagne VL, Martins R, Ourselin S, Rossor MN, Fox NC, Cash DM, Weiner MW, Holtzman DM, Buckles VD, Moulder K, Morris JC. Regional variability of imaging biomarkers in autosomal dominant Alzheimer's disease. Proceedings of the National Academy of Sciences of the United States of America. 2013; 110(47):E4502–4509. [PubMed: 24194552]
10. Sperling RA, Aisen PS, Beckett LA, Bennett DA, Craft S, Fagan AM, Iwatsubo T, Jack CR Jr, Kaye J, Montine TJ, Park DC, Reiman EM, Rowe CC, Siemers E, Stern Y, Yaffe K, Carrillo MC, Thies B, Morrison-Bogorad M, Wagster MV, Phelps CH. Toward defining the preclinical stages of Alzheimer's disease: recommendations from the National Institute on Aging-Alzheimer's Association workgroups on diagnostic guidelines for Alzheimer's disease. Alzheimer's & dementia: the journal of the Alzheimer's Association. 2011; 7(3):280–292.
11. Morris JC, Aisen PS, Bateman RJ, Benzinger TL, Cairns NJ, Fagan AM, Ghetti B, Goate AM, Holtzman DM, Klunk WE, McDade E, Marcus DS, Martins RN, Masters CL, Mayeux R, Oliver A, Quaid K, Ringman JM, Rossor MN, Salloway S, Schofield PR, Selsor NJ, Sperling RA, Weiner MW, Xiong C, Moulder KL, Buckles VD. Developing an international network for Alzheimer research: The Dominantly Inherited Alzheimer Network. Clin Investig (Lond). 2012; 2(10):975–984.
12. Fagan AM, Csernansky CA, Morris JC, Holtzman DM. The search for antecedent biomarkers of Alzheimer's disease. Journal of Alzheimer's disease: JAD. 2005; 8(4):347–358. [PubMed: 16556966]
13. Reiman EM, Langbaum JB, Tariot PN, Lopera F, Bateman RJ, Morris JC, Sperling RA, Aisen PS, Roses AD, Welsh-Bohmer KA, Carrillo MC, Weninger S. CAP--advancing the evaluation of preclinical Alzheimer disease treatments. Nature reviews Neurology. 2016; 12(1):56–61. [PubMed: 26416539]
14. Ikonomovic MD, Klunk WE, Abrahamson EE, Mathis CA, Price JC, Tsopelas ND, Lopresti BJ, Ziolko S, Bi W, Paljug WR, Debnath ML, Hope CE, Isanski BA, Hamilton RL, DeKosky ST. Post-mortem correlates of in vivo PiB-PET amyloid imaging in a typical case of Alzheimer's disease. Brain. 2008; 131(Pt 6):1630–1645. [PubMed: 18339640]
15. Klunk WE, Engler H, Nordberg A, Wang Y, Blomqvist G, Holt DP, Bergstrom M, Savitcheva I, Huang GF, Estrada S, Ausen B, Debnath ML, Barletta J, Price JC, Sandell J, Lopresti BJ, Wall A, Koivisto P, Antoni G, Mathis CA, Langstrom B. Imaging brain amyloid in Alzheimer's disease with Pittsburgh Compound-B. Annals of neurology. 2004; 55(3):306–319. [PubMed: 14991808]
16. Price JC, Klunk WE, Lopresti BJ, Lu X, Hoge JA, Ziolko SK, Holt DP, Meltzer CC, DeKosky ST, Mathis CA. Kinetic modeling of amyloid binding in humans using PET imaging and Pittsburgh Compound-B. Journal of cerebral blood flow and metabolism: official journal of the International Society of Cerebral Blood Flow and Metabolism. 2005; 25(11):1528–1547.
17. Braak H, Braak E. Neuropathological stageing of Alzheimer-related changes. Acta neuropathologica. 1991; 82(4):239–259. [PubMed: 1759558]
18. Mitchell TW, Mufson EJ, Schneider JA, Cochran EJ, Nissanov J, Han LY, Bienias JL, Lee VM, Trojanowski JQ, Bennett DA, Arnold SE. Parahippocampal tau pathology in healthy aging, mild cognitive impairment, and early Alzheimer's disease. Annals of neurology. 2002; 51(2):182–189. [PubMed: 11835374]
19. Hyman BT, Van Hoesen GW, Damasio AR, Barnes CL. Alzheimer's disease: cell-specific pathology isolates the hippocampal formation. Science. 1984; 225(4667):1168–1170. [PubMed: 6474172]
20. Arnold SE, Hyman BT, Flory J, Damasio AR, Van Hoesen GW. The topographical and neuroanatomical distribution of neurofibrillary tangles and neuritic plaques in the cerebral cortex of patients with Alzheimer's disease. Cerebral cortex. 1991; 1(1):103–116. [PubMed: 1822725]
21. Price JL, Morris JC. Tangles and plaques in nondemented aging and "preclinical" Alzheimer's disease. Annals of neurology. 1999; 45(3):358–368. [PubMed: 10072051]

22. Thangavel R, Van Hoesen GW, Zaheer A. Posterior parahippocampal gyrus pathology in Alzheimer's disease. Neuroscience. 2008; 154(2):667–676. [PubMed: 18486350]

23. Schuff N, Woerner N, Boreta L, Kornfield T, Shaw LM, Trojanowski JQ, Thompson PM, Jack CR Jr, Weiner MW. Alzheimer's Disease Neuroimaging I. MRI of hippocampal volume loss in early Alzheimer's disease in relation to ApoE genotype and biomarkers. Brain. 2009; 132(Pt 4):1067–1077. [PubMed: 19251758]

24. Jack CR Jr, Petersen RC, Xu Y, O'Brien PC, Smith GE, Ivnik RJ, Boeve BF, Tangalos EG, Kokmen E. Rates of hippocampal atrophy correlate with change in clinical status in aging and AD. Neurology. 2000; 55(4):484–489. [PubMed: 10953178]

25. Price JL, Ko AI, Wade MJ, Tsou SK, McKeel DW, Morris JC. Neuron number in the entorhinal cortex and CA1 in preclinical Alzheimer disease. Archives of neurology. 2001; 58(9):1395–1402. [PubMed: 11559310]

26. Gomez-Isla T, Price JL, McKeel DW Jr, Morris JC, Growdon JH, Hyman BT. Profound loss of layer II entorhinal cortex neurons occurs in very mild Alzheimer's disease. The Journal of neuroscience: the official journal of the Society for Neuroscience. 1996; 16(14):4491–4500. [PubMed: 8699259]

27. Juottonen K, Lehtovirta M, Helisalmi S, Riekkinen PJ Sr, Soininen H. Major decrease in the volume of the entorhinal cortex in patients with Alzheimer's disease carrying the apolipoprotein E epsilon4 allele. J Neurol Neurosurg Psychiatry. 1998; 65(3):322–327. [PubMed: 9728943]

28. Dickerson BC, Stoub TR, Shah RC, Sperling RA, Killiany RJ, Albert MS, Hyman BT, Blacker D, Detoledo-Morrell L. Alzheimer-signature MRI biomarker predicts AD dementia in cognitively normal adults. Neurology. 2011; 76(16):1395–1402. [PubMed: 21490323]

29. Benveniste H, Einstein G, Kim KR, Hulette C, Johnson GA. Detection of neuritic plaques in Alzheimer's disease by magnetic resonance microscopy. Proceedings of the National Academy of Sciences. 1999; 96(24):14079–14084.

30. Meadowcroft MD, Connor JR, Smith MB, Yang QX. MRI and histological analysis of beta-amyloid plaques in both human Alzheimer's disease and APP/PS1 transgenic mice. Journal of Magnetic Resonance Imaging. 2009; 29(5):997–1007. [PubMed: 19388095]

31. Wengenack TM, Reyes DA, Curran GL, Borowski BJ, Lin J, Preboske GM, Holasek SS, Gilles EJ, Chamberlain R, Marjanska M, Jack CR Jr, Garwood M, Poduslo JF. Regional differences in MRI detection of amyloid plaques in AD transgenic mouse brain. NeuroImage. 2011; 54(1):113–122. [PubMed: 20728546]

32. Chamberlain R, Reyes D, Curran GL, Marjanska M, Wengenack TM, Poduslo JF, Garwood M, Jack CR. Comparison of amyloid plaque contrast generated by T2-weighted, T 2*-weighted, and susceptibility-weighted imaging methods in transgenic mouse models of Alzheimer's disease. Magnetic Resonance in Medicine. 2009; 61(5):1158–1164. [PubMed: 19253386]

33. Lee S-P, Falangola MF, Nixon RA, Duff K, Helpern JA. Visualization of β-amyloid plaques in a transgenic mouse model of Alzheimer's disease using MR microscopy without contrast reagents. Magnetic Resonance in Medicine. 2004; 52(3):538–544. [PubMed: 15334572]

34. Maier FC, Keller MD, Bukala D, Bender B, Mannheim JG, Brereton IM, Galloway GJ, Pichler BJ. Quantification of beta-Amyloidosis and rCBF with Dedicated PET, 7 T MR Imaging, and High-Resolution Microscopic MR Imaging at 16. 4 T in APP23 Mice. Journal of nuclear medicine: official publication, Society of Nuclear Medicine. 2015; 56(10):1593–1599.

35. Sati P, Cross AH, Luo J, Hildebolt CF, Yablonskiy DA. In vivo quantitative evaluation of brain tissue damage in multiple sclerosis using gradient echo plural contrast imaging technique. NeuroImage. 2010; 51(3):1089–1097. [PubMed: 20338247]

36. Luo J, Jagadeesan BD, Cross AH, Yablonskiy DA. Gradient Echo Plural Contrast Imaging - Signal model and derived contrasts: T2*, T1, Phase, SWI, T1f, FST2*and T2*-SWI. NeuroImage. 2012; 60(2):1073–1082. [PubMed: 22305993]

37. Ulrich X, Yablonskiy DA. Separation of cellular and BOLD contributions to T2* signal relaxation. Magn Reson Med. 2015

38. Zhao Y, Wen J, Cross AH, Yablonskiy DA. On the relationship between cellular and hemodynamic properties of the human brain cortex throughout adult lifespan. NeuroImage. 2016; 133:417–429. [PubMed: 26997360]

39. Luo J, Yablonskiy DA, Hildebolt CF, Lancia S, Cross AH. Gradient echo magnetic resonance imaging correlates with clinical measures and allows visualization of veins within multiple sclerosis lesions. Mult Scler. 2014; 20(3):349–355. [PubMed: 23836876]
40. Wen J, Cross AH, Yablonskiy DA. On the role of physiological fluctuations in quantitative gradient echo MRI: implications for GEPCI, QSM, and SWI. Magn Reson Med. 2014
41. Wen J, Yablonskiy DA, Luo J, Lancia S, Hildebolt C, Cross AH. Detection and quantification of regional cortical gray matter damage in multiple sclerosis utilizing gradient echo MRI. NeuroImage: Clinical. 2015; 9:164–175. [PubMed: 27330979]
42. Patel KR, Luo J, Alvarez E, Piccio L, Schmidt RE, Yablonskiy DA, Cross AH. Detection of cortical lesions in multiple sclerosis: A new imaging approach. Multiple Sclerosis Journal – Experimental, Translational and Clinical. 2015:1.
43. Mamah D, Wen J, Luo J, Ulrich X, Barch DM, Yablonskiy D. Subcomponents of brain T2* relaxation in schizophrenia, bipolar disorder and siblings: A Gradient Echo Plural Contrast Imaging (GEPCI) study. Schizophr Res. 2015
44. Morris JC. The Clinical Dementia Rating (CDR): current version and scoring rules. Neurology. 1993; 43(11):2412–2414.
45. Johnson DK, Storandt M, Morris JC, Langford ZD, Galvin JE. Cognitive profiles in dementia: Alzheimer disease vs healthy brain aging. Neurology. 2008; 71(22):1783–1789. [PubMed: 19029518]
46. Mintun MA, Larossa GN, Sheline YI, Dence CS, Lee SY, Mach RH, Klunk WE, Mathis CA, DeKosky ST, Morris JC. [11C]PIB in a nondemented population: potential antecedent marker of Alzheimer disease. Neurology. 2006; 67(3):446–452. [PubMed: 16894106]
47. Yablonskiy DA, Sukstanskii AL, Luo J, Wang X. Voxel spread function method for correction of magnetic field inhomogeneity effects in quantitative gradient-echo-based MRI. Magn Reson Med. 2013; 70(5):1283–1292. [PubMed: 23233445]
48. Mugler JP, Brookeman JR. Three-dimensional magnetization-prepared rapid gradient-echo imaging (3D MP RAGE). Magnetic Resonance in Medicine. 1990; 15(1):152–157. [PubMed: 2374495]
49. Quirk JD, Sukstanskii AL, Bretthorst GL, Yablonskiy DA. Optimal decay rate constant estimates from phased array data utilizing joint Bayesian analysis. J Magn Reson. 2009; 198(1):49–56. [PubMed: 19181549]
50. Yablonskiy DA. Quantitation of intrinsic magnetic susceptibility-related effects in a tissue matrix. Phantom study Magnetic Resonance in Medicine. 1998; 39(3):417–428. [PubMed: 9498598]
51. Yablonskiy DA, Haacke EM. Theory of NMR signal behavior in magnetically inhomogeneous tissues: the static dephasing regime. Magn Reson Med. 1994; 32(6):749–763. [PubMed: 7869897]
52. Vlassenko AG, Vaishnavi SN, Couture L, Sacco D, Shannon BJ, Mach RH, Morris JC, Raichle ME, Mintun MA. Spatial correlation between brain aerobic glycolysis and amyloid-beta (Abeta) deposition. Proceedings of the National Academy of Sciences of the United States of America. 2010; 107(41):17763–17767. [PubMed: 20837517]
53. Duyn JH. The future of ultra-high field MRI and fMRI for study of the human brain. NeuroImage. 2012; 62(2):1241–1248. [PubMed: 22063093]
54. Wang X, Sukstanskii AL, Yablonskiy DA. Optimization strategies for evaluation of brain hemodynamic parameters with qBOLD technique. Magn Reson Med. 2013; 69(4):1034–1043. [PubMed: 22623013]
55. Reuter M, Schmansky NJ, Rosas HD, Fischl B. Within-subject template estimation for unbiased longitudinal image analysis. NeuroImage. 2012; 61(4):1402–1418. [PubMed: 22430496]
56. Jenkinson M, Beckmann CF, Behrens TEJ, Woolrich MW, Smith SM. FSL. NeuroImage. 2012; 62(2):782–790. [PubMed: 21979382]
57. Jenkinson M, Bannister P, Brady M, Smith S. Improved Optimization for the Robust and Accurate Linear Registration and Motion Correction of Brain Images. Neuroimage. 2002; 17(2):825–841. [PubMed: 12377157]
58. Yablonskiy, DA. Quntitative T2 contrast with Gradient Echoes. 8th Annual Meeting of the International Society for Magnetic Resonance in Medicine; Denver, Colorado. 2000.

59. He X, Zhu M, Yablonskiy DA. Validation of oxygen extraction fraction measurement by qBOLD technique. Magn Reson Med. 2008; 60(4):882–888. [PubMed: 18816808]
60. Benjamini Y, Hochberg Y. Controlling the False Discovery Rate: A Practical and Powerful Approach to Multiple Testing. Journal of the Royal Statistical Society Series B (Methodological). 1995; 57(1):289–300.
61. Hoesen, GWV. The human parahippocampal region in Alzheimer's disease, dementia, and ageing. In: Witter, MP., Wouterlood, FG., editors. The parahippocampal region: organization and role in cognitive function. Oxford; New York: Oxford University Press; 2002.
62. Scharfman HE, Witter MP, Schwarcz R. Preface. Annals of the New York Academy of Sciences. 2000; 911(1):ix–xiii. [PubMed: 10911863]
63. Su Y, D'Angelo GM, Vlassenko AG, Zhou G, Snyder AZ, Marcus DS, Blazey TM, Christensen JJ, Vora S, Morris JC, Mintun MA, Benzinger TL. Quantitative analysis of PiB-PET with FreeSurfer ROIs. PloS one. 2013; 8(11):e73377. [PubMed: 24223109]
64. Raichle ME, MacLeod AM, Snyder AZ, Powers WJ, Gusnard DA, Shulman GL. A default mode of brain function. Proceedings of the National Academy of Sciences of the United States of America. 2001; 98(2):676–682. [PubMed: 11209064]
65. Fjell AM, McEvoy L, Holland D, Dale AM, Walhovd KB. What is normal in normal aging? Effects of aging, amyloid and Alzheimer's disease on the cerebral cortex and the hippocampus Progress in neurobiology. 2014; 117:20–40. [PubMed: 24548606]
66. Buckner RL, Snyder AZ, Shannon BJ, LaRossa G, Sachs R, Fotenos AF, Sheline YI, Klunk WE, Mathis CA, Morris JC, Mintun MA. Molecular, structural, and functional characterization of Alzheimer's disease: evidence for a relationship between default activity, amyloid, and memory. The Journal of neuroscience: the official journal of the Society for Neuroscience. 2005; 25(34): 7709–7717. [PubMed: 16120771]
67. Morris JC, Roe CM, Grant EA, Head D, Storandt M, Goate AM, Fagan AM, Holtzman DM, Mintun MA. Pittsburgh compound B imaging and prediction of progression from cognitive normality to symptomatic Alzheimer disease. Archives of neurology. 2009; 66(12):1469–1475. [PubMed: 20008650]
68. Price JL, McKeel DW Jr, Buckles VD, Roe CM, Xiong C, Grundman M, Hansen LA, Petersen RC, Parisi JE, Dickson DW, Smith CD, Davis DG, Schmitt FA, Markesbery WR, Kaye J, Kurlan R, Hulette C, Kurland BF, Higdon R, Kukull W, Morris JC. Neuropathology of nondemented aging: presumptive evidence for preclinical Alzheimer disease. Neurobiology of aging. 2009; 30(7): 1026–1036. [PubMed: 19376612]
69. Elman JA, Oh H, Madison CM, Baker SL, Vogel JW, Marks SM, Crowley S, O'Neil JP, Jagust WJ. Neural compensation in older people with brain amyloid-beta deposition. Nature neuroscience. 2014; 17(10):1316–1318. [PubMed: 25217827]
70. Rentz DM, Locascio JJ, Becker JA, Moran EK, Eng E, Buckner RL, Sperling RA, Johnson KA. Cognition, reserve, and amyloid deposition in normal aging. Annals of neurology. 2010; 67(3): 353–364. [PubMed: 20373347]
71. Wirth M, Madison CM, Rabinovici GD, Oh H, Landau SM, Jagust WJ. Alzheimer's disease neurodegenerative biomarkers are associated with decreased cognitive function but not beta-amyloid in cognitively normal older individuals. The Journal of neuroscience: the official journal of the Society for Neuroscience. 2013; 33(13):5553–5563. [PubMed: 23536070]

Highlights

- Alzheimer disease (AD) affects at least 5 million individuals in the USA alone
- GEPCI is a MRI-based approach to the *in vivo* evaluation of AD pathology
- GEPCI metrics are good correlates of amyloid accumulation and neurodegeneration
- GEPCI metrics differentiate normal individuals and those with asymptomatic and early AD

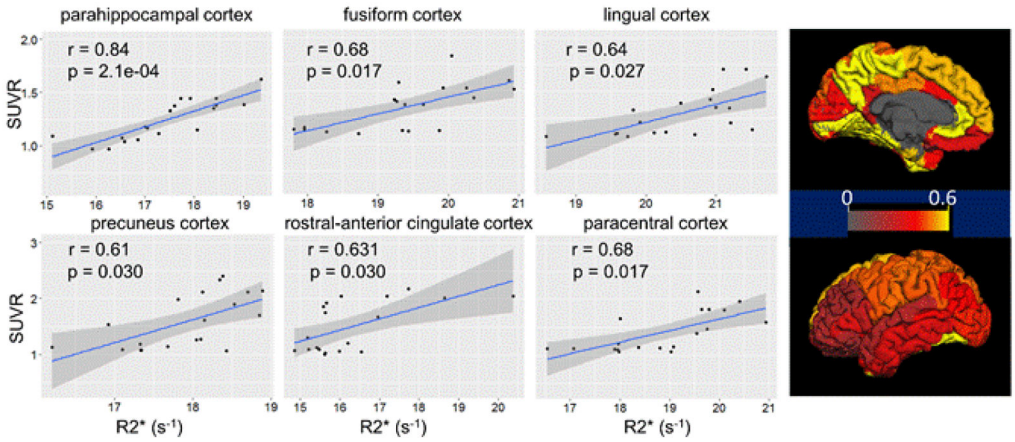

Figure 1.

Correlation between PET PiB Aβ SUVR (dimensionless) and R2* (s^{-1}) relaxation rate constant obtained in 19 participants. Plots show examples of correlation in several brain regions. Each point represents a single participant. Shaded areas represent 95% confidence intervals of the linear fits (solid lines). Pearson correlation coefficients (r) and p values (corrected for multiple comparison using false discovery rate over all cortical regions) are shown in the left upper corners. The surface maps on the right represent r values in all cortical areas. The image segmentation is based on the FreeSurfer software (55). The data show significant correlations not only in the areas of high Aβ accumulation (e.g. precuneus) but also in the areas of MTL, such as the parahippocampal cortex and the fusiform cortex. Remarkably, the strongest and most significant correlation exists in the parahippocampal cortex – the area of low Aβ accumulation.

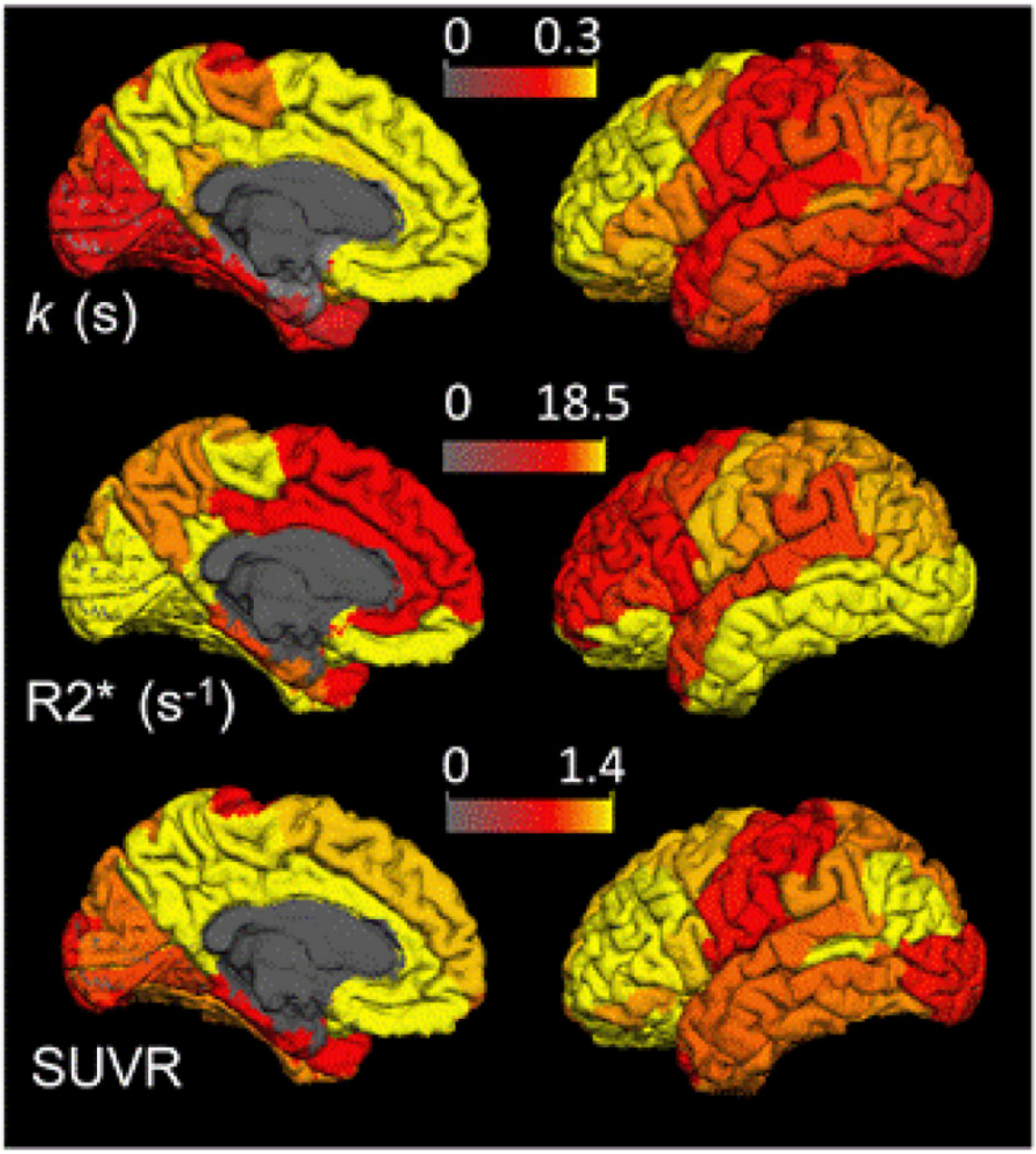

Figure 2.

Upper row represents the surface maps of the slopes (units of sec) of linear regression (coefficient k in Eq. [4]) between regional PET-measured Aβ SUVR and parahippocampal R2* across 19 participants. All regional slopes are positive. The coefficients of the linear regressions are listed in Table 1. The second and the last rows represent the averaged cortical mean values of R2* and Aβ SUVR across the same 19 participants. White matter, deep gray matter and ventricles were excluded. The image segmentation is based on the FreeSurfer software (55).

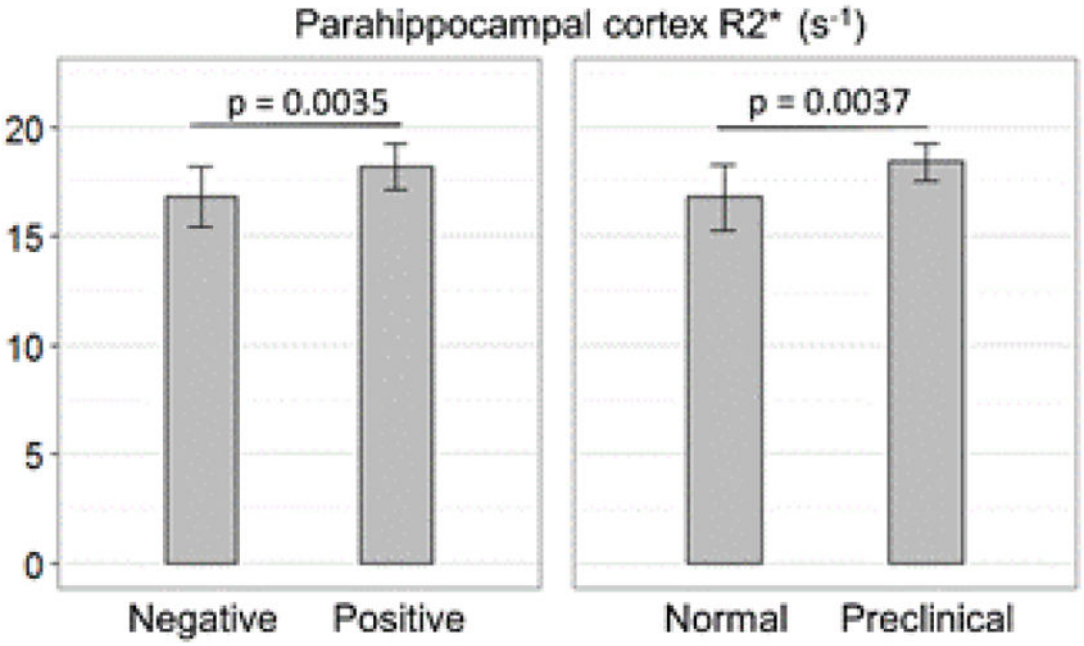

Figure 3.

Group comparison based on the R2 *measurements in the parahippocampal cortex. The bar graph on the left shows significant differences between all participants (independent of CDR) with negative (n = 15, R2* = 16.79 ± 1.40 s^{-1}) and positive (n = 19, R2* = 18.20 ± 1.08 s^{-1}) Aβ status (see definition in the Methods). The bar graph on the right shows significant differences between normal group (CDR = 0, Aβ negative, n=13, R2* = 16.77 ± 1.51 s^{-1}) and preclinical group (CDR = 0, Aβ positive, n = 10, R2* = 18.41 ± 0.84 s^{-1}).

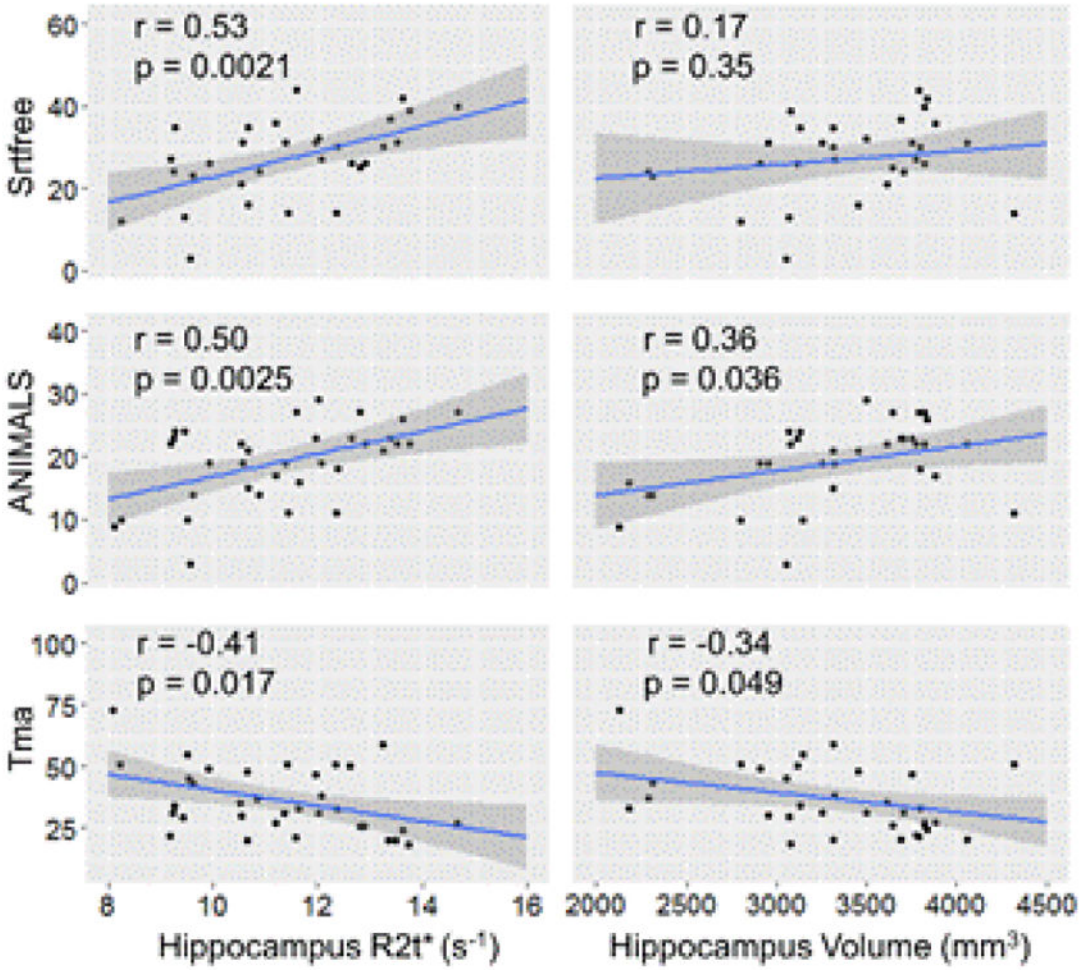

Figure 4.

Correlation between cognitive tests performance and hippocampal R2t*. Cognitive measures included Free and Cued Selective Reminding Test (Srtfree), Animal Naming (ANIMALS), and Trail making Test Part A completion time (Tma). Note that higher scores on Tma indicate worse performance. Correlations with hippocampal volume are also presented for comparison. Each point represents a single participant (n = 34). Shaded areas represent 95% confidence intervals of linear fits (solid lines). Pearson correlation coefficients (r) and p values are shown in the left upper corners.

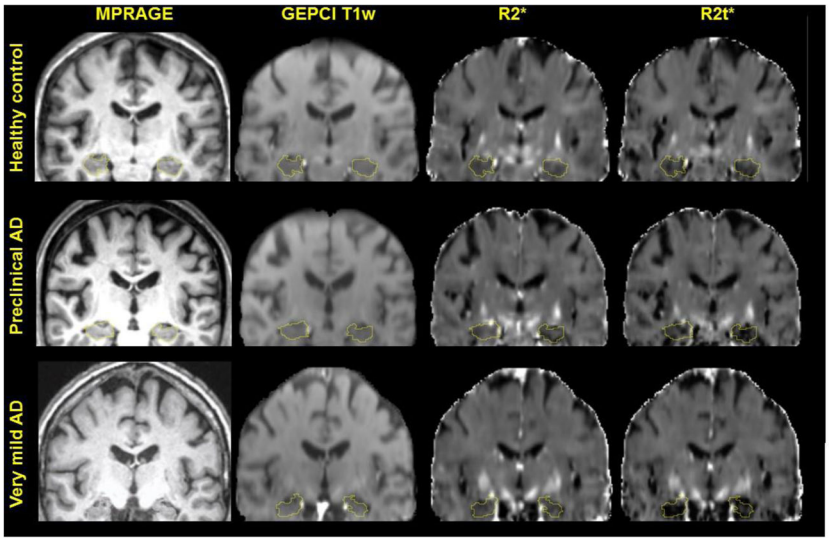

Figure 5.

Examples of images obtained from three participants – 69 year old female representing control group (upper row), 72 year old male representing preclinical AD group (second row) and 69 year old male representing mild AD (CDR = 0.5) group. Thin yellow contours outline hippocampal area determined by FreeSurfer segmentation. In all cases, MPRAGE and GEPCI T1w images show small atrophy progressing from healthy to AD group. Gradually decreased GEPCI R2t* suggest altered tissue integrity even in the preserved hippocampal area.

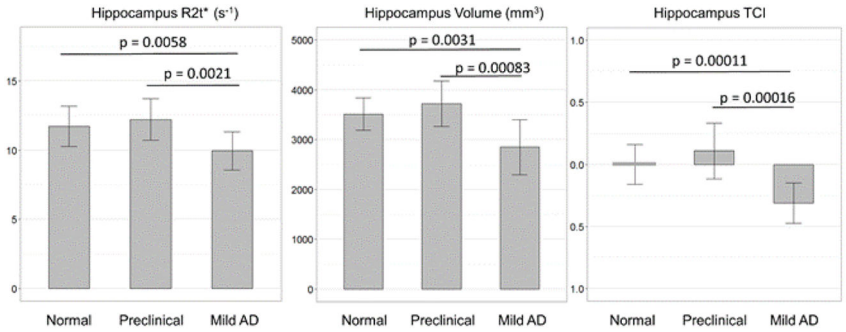

Figure 6.

Bar graphs show the data obtained in the hippocampus of 34 participants. Bars represent mean values and error bars are standard deviations. Data are separated into three groups: Normal, preclinical AD, and mild AD (CDR 0.5 or 1). GEPCI R2t*, and volumes are shown. Also shown is the parameter TCI (tissue content index, Eq.[5]). While R2t* can serve as a surrogate marker of neuronal density/integrity, the TCI can serve as a surrogate marker characterizing a change in the total neuronal content. The results are summarized in Table 2.

Table 1

The results of linear regression analysis of the relationship between regional amyloid SUVR in different cortical regions and the parahippocampal R2*. Cortical regions are selected based on the FreeSurfer segmentation (55). The data show coefficients of linear regression (Eq. [4]) and the correlation coefficients (*r*). The mean value of R2* in the parahippocampal region for the control group in Eq. [4] is 16.55 sec^{-1}.

Cortical area	Intercept (*a*)	Slope (*k*, sec)	p value	r
bankssts	1.35	0.24	2.47E-04	0.75
caudal-anteriorcingulate	1.23	0.27	2.45E-04	0.75
caudal-middlefrontal	1.16	0.24	1.76E-04	0.76
cuneus	1.22	0.12	2.79E-02	0.50
entorhinal	1.10	0.08	1.33E-04	0.77
frontalpole	1.07	0.30	5.31E-04	0.72
fusiform	1.21	0.15	2.02E-04	0.75
inferiorparietal	1.21	0.23	4.08E-04	0.73
inferiortemporal	1.15	0.20	4.63E-04	0.72
insula	1.23	0.18	2.90E-04	0.74
isthmuscingulate	1.34	0.25	5.46E-04	0.72
lateraloccipital	1.15	0.12	1.22E-03	0.68
lateralorbitofrontal	1.26	0.25	4.45E-04	0.72
lingual	1.19	0.12	6.46E-03	0.60
medialorbitofrontal	1.23	0.32	2.98E-04	0.74
middletemporal	1.13	0.21	1.73E-04	0.76
paracentral	1.21	0.23	1.00E-03	0.69
parahippocampal	1.11	0.15	6.09E-06	0.84
parsopercularis	1.19	0.23	4.66E-04	0.72
parsorbitalis	1.13	0.26	4.97E-04	0.72
parstriangularis	1.20	0.24	3.90E-04	0.73
pericalcarine	1.27	0.14	2.56E-02	0.51
postcentral	1.07	0.15	2.02E-03	0.66
posteriorcingulate	1.29	0.32	4.58E-04	0.72
precentral	1.14	0.14	9.57E-04	0.70
precuneus	1.30	0.32	5.93E-04	0.71
rostralanteriorcingulate	1.23	0.31	2.28E-04	0.75
rostralmiddlefrontal	1.16	0.30	4.34E-04	0.73
superiorfrontal	1.14	0.28	3.25E-04	0.74
superiorparietal	1.15	0.21	6.31E-04	0.71
superiortemporal	1.15	0.18	2.45E-04	0.75
supramarginal	1.16	0.21	6.68E-04	0.71
temporalpole	1.11	0.10	9.94E-04	0.69
transversetemporal	1.21	0.18	4.48E-04	0.72

Table 2

The mean and standard deviations of R2t*, volume and TCI in hippocampus over three groups presented in Figure 6.

	R2t*(s^{-1})	Volume(mm^3)	TCI
Normal	11.71 ± 1.45	3512 ± 327	0.00 ± 0.16
Preclinical	12.20 ± 1.50	3720 ± 452	0.11 ± 0.22
Mild AD	9.94 ± 1.38	2849 ± 552	−0.31 ± 0.16

Table 3

Distribution of participants between groups and their demographic information. Note that nine participants in Mild AD group were Aβ positive and two were Aβ negative.

	Normal	Preclinical AD	Mild AD
	CDR=0 Aβ negative	CDR=0 Aβ positive	CDR=0.5 or 1
N	13	10	11 (7/4)
Age	69.6±8.7	72.3±8.4	76.0±8.4
Female/Male	7/6	4/6	3/8